SuperWASP-N extrasolar planet candidates between 18 <RA <21h

Street, R. A., Christian, D. J., Clarkson, W. I., Collier-Cameron, A., Enoch, B., Kane, S. R., ... Barnes, J. (2007). SuperWASP-N extrasolar planet candidates between 18 . DOI: 10.1111/j.1365-2966.2007.11987.x

Document Version:
Publisher's PDF, also known as Version of record

Queen's University Belfast - Research Portal:
[Link to publication record in Queen's University Belfast Research Portal](#)

SuperWASP-N extrasolar planet candidates between 18 < RA < 21 h

R. A. Street,[1,2,3]★ D. J. Christian,[1] W. I. Clarkson,[4,5] A. Collier Cameron,[6]
B. Enoch,[4] S. R. Kane,[6,7] T. A. Lister,[2,6,8] R. G. West,[9] D. M. Wilson,[8] A. Evans,[8]
A. Fitzsimmons,[1] C. A. Haswell,[4] C. Hellier,[8] S. T. Hodgkin,[10] K. Horne,[6] J. Irwin,[10]
F. P. Keenan,[1] A. J. Norton,[4] J. Osborne,[9] D. L. Pollacco,[1] R. Ryans,[1] I. Skillen,[11]
P. J. Wheatley[12] and J. Barnes[6,13]

[1]*Astrophysics Research Centre, Department of Physics and Astronomy, Queen's University Belfast, Belfast BT7 1NN*
[2]*Las Cumbres Observatory, 6740B Cortona Drive, Goleta, CA 93117, USA*
[3]*Department of Physics, Broida Hall, University of California, Santa Barbara, CA 93106-9530, USA*
[4]*Department of Physics & Astronomy, The Open University, Milton Keynes MK7 6AA*
[5]*Space Telescope Science Institute (STScI), 3700 San Martin Drive, Baltimore, MD 21218, USA*
[6]*School of Physics & Astronomy, University of St. Andrews, North Haugh, St. Andrews, Fife KY16 9SS*
[7]*Dept. of Astronomy, University of Florida, 211 Bryant Space Science Center, Gainesville, FL 32611-2055, USA*
[8]*Astrophysics Group, School of Chemistry & Physics, Keele University, Staffordshire ST5 5BG*
[9]*Department of Physics & Astronomy, University of Leicester, Leicester LE1 7RH*
[10]*Institute of Astronomy, University of Cambridge, Madingley Road, Cambridge CB3 0HA*
[11]*Isaac Newton Group of Telescopes, Apartado de correos 321, E-38700 Santa Cruz de la Palma, Tenerife, Spain*
[12]*Department of Physics, University of Warwick, Coventry CV4 7AL*
[13]*Centre for Astrophysics Research, Science & Technology Research Institute, University of Hertfordshire, Hatfield AL10 9AB*

ABSTRACT

The SuperWASP-I (Wide Angle Search for Planets-I) instrument observed 6.7 million stars between 8 and 15 mag from La Palma during the 2004 May–September season. Our transit-hunting algorithm selected 11 626 objects from the 184 442 stars within the RA (right ascension) range 18–21 h. We describe our thorough selection procedure whereby catalogue information is exploited along with careful study of the SuperWASP data to filter out, as far as possible, transit mimics. We have identified 35 candidates which we recommend for follow-up observations.

Key words: techniques: photometric – methods: data analysis – surveys – binaries: eclipsing – planetary systems.

1 INTRODUCTION

The ∼200 exoplanets found to date have revolutionized our understanding of how planetary systems form and evolve (Lin, Bodenheimer & Richardson 1996; Burrows et al. 2000). In particular, the discovery of 'hot Jupiters' – Jovian-mass planets in orbits of period ⩽5 d where conditions are too hot for them to have formed – led to a re-evaluation of the theory of orbital migration (Ipatov 1993; Lin et al. 1996). This class of planets have a comparatively high (∼10 per cent) probability of transiting across the face of their parent star. Transiting exoplanets are highly sought-after as an exceptional range of information can be derived from them; to date 19[1] systems have been discovered. Unambiguous measurements of their physical and orbital parameters can be made, thereby providing quantitative data against which to test evolutionary models (e.g. Chabrier et al. 2004). Research into the brightest transiting systems has, among other ground-breaking advances, detected components of exoplanetary atmospheres (Charbonneau et al. 2002) and trailing exosphere (Vidal-Madjar et al. 2003, 2004), and placed limits on the existence of moons (Brown et al. 2001) and other planets in the same system (Steffen & Agol 2005). For a comprehensive review of this exciting field, see Charbonneau et al. (2007).

In Section 2 we introduce the SuperWASP (Wide Angle Search for Planets) project[2] (Pollacco et al. 2006), a wide-angle photometric survey searching for bright transiting planets. Inevitably, all surveys looking for low-amplitude, periodic eclipses will find those caused by stellar as well as planetary objects. Brown (2003) and O'Donovan et al. (2006) discuss several astrophysical systems which can masquerade as transiting exoplanets. The fact that photometric data alone cannot identify transiting planets conclusively was demonstrated by the OGLE (Optical Gravitational Lensing

★E-mail: rstreet@lcogt.net
[1]The exoplanet encyclopedia, http://exoplanet.eu

[2]www.superwasp.org

Experiment) project (e.g. Udalski et al. 2004), who have found to date 177 eclipsing candidates, of which five have been confirmed as planetary.

We therefore need an effective filtering strategy to eliminate 'false positives' wherever possible in advance of time-consuming follow-up observations. Section 3 describes our system of evaluating candidates to select high-priority objects for follow-up. We discuss the transit candidates discovered within the RA (right ascension) range 18–21 h during SuperWASP-North (SW-N)'s 2004 observing season in Sections 4–6.

2 OBSERVATIONS AND DATA REDUCTION

SW-N at the Isaac Newton Group of Observatories, La Palma, Canary Islands, is a dedicated ultrawide field photometric survey instrument observing northern field stars of $V \sim 8$–15 mag. Our science goals are designed to explore long baseline (months–years) time domain astronomy, in particular the search for transiting exoplanets. The station supported five cameras in 2004, each with a field of view of $7.8° \times 7.8°$. The instrumentation, observing strategy and data reduction pipeline are described in detail in Pollacco et al. (2006).

The fields monitored were carefully selected to avoid the Galactic plane, in contrast to some other transit surveys. The ecliptic plane was also avoided wherever possible to minimize the sky background due to the Moon and to exclude (Solar system) planets. During the 2004 season we acquired light curves for some 6.7 million objects.

A custom-written, fully automated data reduction pipeline, developed by our consortium, has been applied to the 2004 data (see Collier Cameron et al. 2006; Pollacco et al. 2006). The photometric output is stored in, and exploited from, the SuperWASP Data Archive held at the University of Leicester. The pipeline routinely achieves a photometric precision of $\sim$5 mmag for stars with $V \sim$ 9.5, rising to $\sim$0.02 mag at $V \sim$ 13. This gives us a sample of $\sim$1.2 million stars with which to search for transits from SW-N's first season (see Christian et al. 2006; Lister et al. 2006).

2.1 RA range 18–21 h

The HUNTSMAN algorithm (Collier Cameron et al. 2006) was applied to search for transits in the light curves of stars with an rms of $\lesssim$0.02 mag or in practice, those brighter than 13 mag. We note that transits can be detected around late-type stars of fainter magnitudes; these will be the subject of a follow-up paper owing to the computational demands of searching much larger numbers of stars. We further constrain our searches to those stars for which we have at least 500 photometric measurements, spanning a period of $\geqslant$10 nights. In total, 184 442 stars met these conditions within the RA range 18–21 h, and their distribution is summarized in Table 1.

Our ability to detect transiting planets in these data depends on several factors: the spectral types of monitored stars and the numbers for which we achieve adequately precise photometry, the degree of crowding in the fields, our observing window function and length of the data set, and not least, the frequency of hot Jovian exoplanets and the distributions of their periods and other physical parameters.

Brown (2003) presents a thorough discussion of the transit recovery rates expected for wide-field transit surveys, emphasizing that it is a strong function of planetary period for single-site observations such as ours. He also found that the rate of transit recovery depends on the distribution of spectral types surveyed. Early ground-based surveys [e.g. STellar Astrophysics and Research on

Table 1. J2000.0 coordinates of field centres surveyed in this work, giving for each field the number of targets searched by the transit-hunting algorithm, and the number of stars selected by it.

RA (^{h} ^{m} ^{s})	Dec. (° ′ ″)	No. nights	No. targets	No. stars extracted	DAS
18 16 00	+31 26 00	127	19 810	1396	3
18 17 00	+23 26 00	129	24 220	1737	4
18 20 00	+39 23 00	118	16 429	850	4
18 20 00	+47 23 00	116	14 085	1011	3
20 45 00	+09 28 00	97	21 390	1090	1
20 45 00	+16 28 00	5	2 259	90	1
20 45 00	+16 28 00	116	25 971	1226	2
20 46 00	+24 45 00	104	26 873	1669	5
21 14 00	+16 28 00	116	17 747	1220	3
21 15 00	+08 28 00	116	14 225	1200	4
21 15 00	+23 51 00	5	689	55	3
21 16 00	+15 27 00	5	744	82	4
Total			184 442	11 626	

Exoplanets (STARE), Vulcan] concentrated on Galactic plane fields in order to maximize the numbers of stars monitored. While large numbers of stars are crucial to any such survey, the larger populations of early-type main-sequence and giant stars in Galactic plane fields only serve to exacerbate the blending. These stars do not contribute significantly to the detection statistics since transit amplitude is inversely proportional to the stellar radius, making planetary companions difficult to detect.

For this reason, SW-N has deliberately avoided the crowded Galactic plane fields, relying instead on our ultrawide field of view to gather sufficient numbers of stars. Fig. 1(a) provides a census of the spectral types covered by our data from a representative field (SW 2045+1628), deriving colour information for each star from the Two Micron All Sky Survey (2MASS) catalogue. Main-sequence stars make up the dominant peak ($J - K < 0.5$) in the SW-N sample. To complement this, Fig. 1(b) presents the colour–colour diagram for the same data, extending from $\sim$late-A/early-F stars down to approximately early-M type and showing a cluster of points around the solar values of $J - H \sim 0.3$, $H - K \sim 0.1$.

Pont, Zucker & Queloz (2006) highlighted the detrimental effect of residual systematic noise in the photometry of this type of survey. While we have gone to great lengths to minimize these systematics (see Section 3.1), the noise in our data is 'red' rather than 'white'. This has the effect of raising the signal-to-noise ratio (S/N) required to detect transiting systems (Smith et al. 2006 investigate the implications for our survey characteristics in detail). In practical terms, an observer must obtain longer baseline data including larger numbers of transits to boost the S/N.

To illustrate this, Fig. 2 demonstrates the probability of detecting N_t or more transits as a function of orbital period, P, from the data obtained for several fields illustrating the range of observation intervals spanned in this data set. A transit is counted as 'observed' if data were obtained within the phase range of $\phi < 0.1w/P$ or $\phi > 1 - 0.1w/P$, where w is the expected transit duration, estimated from $w \sim [(PR_*)/(\pi a)]$, where the separation, a, is calculated from Kepler's third law. All cases assumed the host star to be a dwarf star of mass $0.9 \, M_\odot$ and radius $R_* = 0.9 \, R_\odot$.

SW produces well-sampled data of acceptable quality most nights and generally $\gtrsim$40 per cent of a given transit is observed during a detectable event. Setting a detection threshold of only three transits, our data returns 100 per cent of all transiting systems for almost
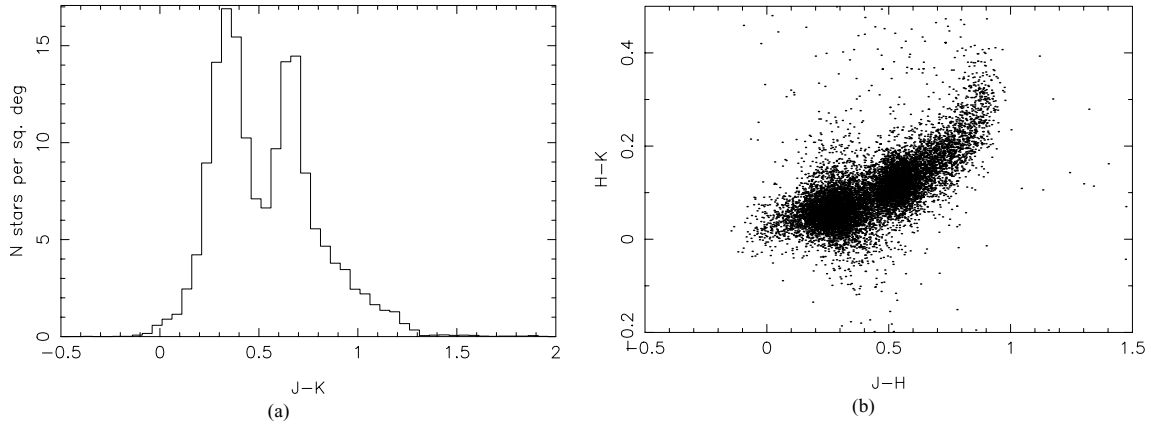
Figure 1. A census of the population of stars monitored in RA = 18–21 h. The colour information is derived from the 2MASS catalogue.
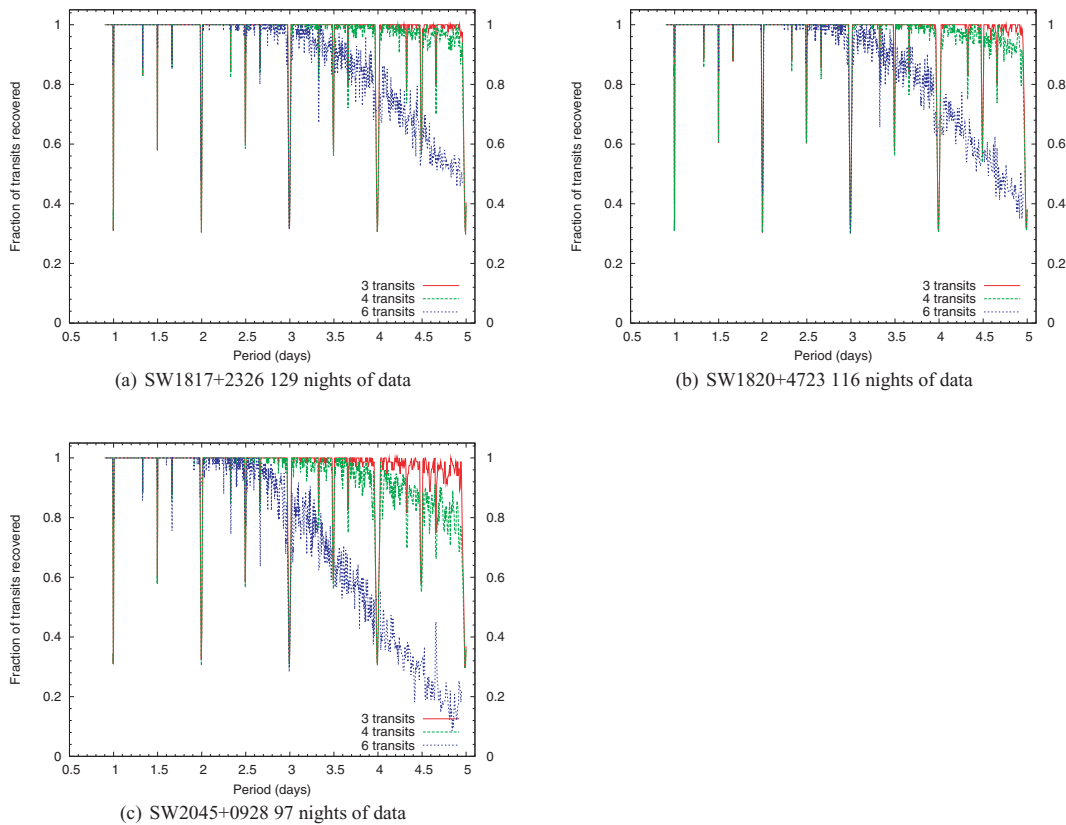
Figure 2. Probabilities of observing more than N_t transits from the 2004 SW-N data for fields within the range RA = 18–21 h, as a function of the planetary orbital period.

all orbital periods up to ∼5 d. As our observations contain daytime gaps, the probability of identifying systems with periods close to an integer multiples of 1 or 1.5 d is only ∼35 per cent. The recovery rate also drops for $P \geqslant 4$ d, implying a longer time-base of observations is required. This is particularly noticeable in the SW 2045+0928 field, which has the shortest time-base. When the required number of transits is increased to six, the detectable planets are confined to shorter periods ($\leqslant 3$ d). Two fields in the RA range, SW 2115+0828 and SW 2116+1527, have significantly less data than the others: 5 nights in total (spread over >10 nights). They were included in the search automatically as they pass the data criteria, but produced understandably fewer candidates.

3 THE CANDIDATE SELECTION PROCEDURE

3.1 Stage 1: the HUNTSMAN transit finding package

Collier Cameron et al. (2006) present a detailed discussion of the corrections applied to the SW-N photometry and the nature of the adapted-box-fitting least squares transit-hunting algorithm employed here. It produces a 'periodogram' of the difference in the goodness-of-fit statistic $\Delta \chi^2$ between each model relative to the no-transit case, plotted against transit frequency.

HUNTSMAN rejects obviously variable stars with $\chi^2 > 3.5N$ ($N =$ number of data points), those less than two transits, and those

solutions which have phase gaps in the folded light curve greater than 2.5 times the transit duration. A candidate's signal-to-red noise ratio, S_{red}, must be greater than 5.0, taking account of the dominance of systematics in the photometric noise (Pont et al. 2006). The strongest peaks in the $\Delta\chi^2$ periodogram corresponding to brightening and dimming are used to define the 'antitransit ratio' (Burke et al. 2006), $\Delta\chi^2/\Delta\chi_-^2$. Candidates must have $\Delta\chi^2/\Delta\chi_-^2 > 1.5$. The algorithm also estimates the degree of ellipsoidal variation in the out-of-transit light curve by producing a signal-to-noise statistic, S/N_{ellip}.

HUNTSMAN selected 11 626 candidates in total from the fields in this data set, summarized in Table 1. In the next section we describe the subsequent stages of systematic candidate assessment employed to eliminate interlopers.

3.2 Stage 2: visual assessment of light curves

A visual inspection was made of each light curve in conjunction with the corresponding periodogram of $\Delta\chi^2$ plotted against frequency. For a candidate to be selected, it had to display a clear transit with credible amplitude, width and period and a smoothly sampled folded light curve. Our finite-length, single-site observations meant that light curves folded on multiples of 1 d were by far the most common transit mimic. The vast majority of these cases were rapidly eliminated on sight as they showed no clear transit signal. Many classes of obvious stellar binaries or variables were also removed from the candidate list.

We developed the following four-digit coding scheme to try to quantify this subjective inspection process as far as possible.

(i) Digit 1: shape and visibility of the transit.

    (a) Clear transit-shaped signal of credible width and depth.

    (b) Shallow/noisy but clearly visible transit signal.

    (c) Transit barely visible, either very shallow, lost in noise or ill shaped.

    (d) Partial transit or gaps around phase 0 but still showing clear transit morphology.

    (e) Signs of a dip at phase 0 but no clear in/egress.

(ii) Digit 2: out-of-transit light curve.

    (a) Clean and flat, no other variations.

    (b) Noisy but flat.

    (c) Signs of ellipsoidal variation or suspected secondary eclipses (includes some candidates which have been folded on twice the period).

    (d) Shows low-amplitude sinusoidal variation on short time-scales, giving a 'knotty' appearance (can indicate that the light curve is folded on the wrong period).

    (e) Realistic variability of some other form out of transit.

    (f) Multilevel or 'jumpy' light curves (can indicate the wrong period or photometry artefacts).

(iii) Digit 3: distribution of points in the folded light curve.

    (a) Smoothly sampled with a similar density of points throughout.

    (b) Some minor regions with slightly lower density of points, retaining a clear signal.

    (c) Significant clumpy of data points (can indicate a pathological period).

(iv) Digit 4: credibility of determined period.

    (a) No reason to doubt measured period, clear peak in $\Delta\chi^2$ periodogram.

    (b) Period gives a secure signal visible in the folded light curve, but peak lies close to a known alias. Sometimes associated with gaps in the folded light curve.

    (c) Signal visible in folded light curve but period is a known alias or peak lies at a commonly occurring frequency.

    (d) Light curve suggests that the measured period is wrong.

We emphasize that this is designed to guide the manual selection of targets, rather than to provide a hard 'statistic' on which a threshold cut might be applied. The code for each star was assessed on a case-by-case basis. That said, stars coded '[4, 5]nnn', 'n[5, 6]nn' or 'nn[3]n' were almost always eliminated unless there were very clear signs of a planet-like transit within the light curve despite its shortcomings. Candidates with '[3]nnn' or 'n[3, 4]nn' were assessed with caution. However, targets with 'n[3]nn' and/or 'nnn[4]' that otherwise showed a clear transit signal were retained and alternative periods were explored.

This process uncovered several exciting, high S/N planetary candidates but inevitably also produced a number of cases close to the threshold. Like all our candidates, such cases were required to have believable transit-like light curves and credible parameters sufficient to pass our criteria. Nevertheless, some stars, while intriguing, only just made the cut. For instance, some objects demonstrated a clear, transit-like light curve, but had a period close to an integer multiple of 1 d. Others were close to the cut-off for ellipsoidal variation. Since objects in this category were potentially low-mass star or brown dwarf binaries and therefore of independent interest, they were retained in the candidate list but not short-listed after stage 4.

3.3 Stage 3: selection criteria

Surviving candidates were subject to the following requirements.

(i) The S_{red} must be at least 8.0.

(ii) The period must be $\geqslant 1.05$ d. This criterion is implemented in order to reject candidates folded on 1-d aliases.

(iii) The number of transits observed must be $\geqslant 3$.

(iv) Antitransit ratio must be greater than 2.0.

(v) The S/N_{ellip} should be less than about 8.0. While this threshold was generally reliable, a number of objects were found which had a value of S/N_{ellip} exceeding this threshold yet the out-of-transit light curve appeared flat to visual inspection. In cases with exceptionally clear, believable transit-like light curves, a degree of human discretion was afforded.

We elected not to search for transits with periods less than 1.05 d as early test runs resulted in unfeasibly large numbers of false alarms folded on periods that are integer fractions of 1 d. It was decided that separate searches would be run for very short (and long) period planets after the present work had cultivated experience in false-positive rejection.

3.4 Stage 4: compilation of catalogue data

Objects surviving this cull were submitted to SW's online Variable Star Investigator tool (Wilson et al. 2007), which performs automated queries on a number of existing photometric catalogues including 2MASS (Skrutskie et al. 2006), Tycho-2 (Høg et al. 2000), SIMBAD (Wenger et al. 2000) and *Hipparcos* (Perryman et al. 1997) among others. This provided for each candidate a table of multicolour photometric information, lists of other nearby objects falling within SW-N's photometric aperture of ~48 arcsec and 3 ×

3 arcmin^2 and Finder Chart from Digitized Sky Survey (Cabanela et al. 2003, DSS;) and 2MASS. The latter information was used to assess the degree to which each star is blended in the SW-N photometry, a major cause of false positives. If a brighter object was found within a candidate's aperture, then that star was removed from the target list.

Two separate temperature–colour relationships were employed to estimate the temperature of each candidate star, assuming it to be main sequence and that the measured colours were not contaminated by light from the companion (as expected under the exoplanet hypothesis). The first relationship uses Tycho-2 V_T and 2MASS K with an uncertainty of 91 K, and the second relationship uses 2MASS J and H (uncertainty 186 K):

$$T_{\mathrm{eff}} = 213.19(V_T - K)^2 - 1920.1(V_T - K) + 8335.7, \tag{1}$$

$$T_{\mathrm{eff}} = -4369.5(J - H) + 7188.2. \tag{2}$$

These were derived from the temperature data on 30 000 FGK dwarf stars presented in Ammons et al. (2006) for which the precision of the Tycho-2 and 2MASS photometry is better than 1 per cent. The use of the second relation, based on infrared (IR) colours, is more sensitive to the presence of cooler companion bodies. A significant discrepancy between the two temperature (and hence radius) estimates can therefore indicate the presence of a companion (often stellar).

The colour indices, together with the USNO-B1.0 proper motions (μ) were also used as an indicator of the luminosity class of the target. The reduced proper motion (RPM$_J$) was computed from

$$\mathrm{RPM}_J = J + 5\log_{10}\mu. \tag{3}$$

Plotted against the $J - H$ index, dwarfs are separated from giants, as they lean towards higher values of RPM$_J$ and low $J - H$. A polynomial boundary was set between the two groups so that VARIABLE STAR INVESTIGATOR (VSI) could issue a warning when this threshold is crossed. Brown (2003) demonstrated that $J - K$ colours can also act as a rough indicator of luminosity based on data from the STARE project. Taking this and Charbonneau et al. (2004) as a guide, *VSI* flags any star with a $J - K > 0.7$ as a possible giant.

The derived T_{eff} values were then used to estimate the spectral type of the host star based on data from Cox (2000) while the radius and mass were estimated using data from Gray (1992). For $T_{\mathrm{eff}} < 7000$ K, the rms of the fit of polynomial functions describing T_{eff} versus radius and mass were 0.016 K in both cases.

A minimum limit on the radius of the companion, R_{p}, was estimated from the stellar radius, R_*, and the transit amplitude, δ, using the relationship derived by Tingley & Sackett (2005) for the I band:

$$R_{\mathrm{c}} \approx \sqrt{\frac{\delta}{1.3}R_*^2}. \tag{4}$$

Our unfiltered, wide bandpass photometry is dominated by the red sensitivity of the CCD and the uncertainty introduced by approximating to I band is smaller than that of the stellar radius estimate.

Although electron degeneracy means that there can be little difference in the radii of objects between $0.5\,\mathrm{M}_\odot$ and $\sim 1\,M_{\mathrm{Jup}}$, we concentrated on objects with predicted R_{p} of less than $\sim 2\,R_{\mathrm{Jup}}$. To aid selection, we also employed the η_{p} diagnostic derived by Tingley & Sackett (2005), comparing the observed transit duration D_{obs} with that theoretically predicted (D_{pred}) for a transiting hot Jupiter:

$$\eta_{\mathrm{p}} = \frac{D_{\mathrm{obs}}}{D_{\mathrm{pred}}} \tag{5}$$

$$= \frac{D_{\mathrm{obs}}}{2Z(1 + \sqrt{1.3/\delta})}\left(\frac{2\pi G\,\mathrm{M}_\odot}{P}\right)^{1/3} R_{\mathrm{c}}^{-(7/12)}\,\mathrm{R}_\odot^{-(5/12)}\left(\frac{1.3}{\delta}\right)^{5/24}, \tag{6}$$

where Z is a factor representing the effects of the projected orbital inclination, set equal to 1 (see discussion in Tingley & Sackett 2005), δ is the depth of the transit and P is the period. Strong exoplanet candidates are expected to have $\eta_{\mathrm{p}} \sim 1$. However, caution was exercised when using this criterion to judge our candidates since the value of R_{p} depends heavily on the value of R_*, the estimate of which is subject to significant uncertainty when made from colour indices alone.

Our assessment of characteristics was quantified using three additional indices from the following coding scheme.

(i) Planetary radius, R_{p}.

$\odot$
    A. $R_{\mathrm{p}} < 1.6\,R_{\mathrm{Jup}}$.
    B. $1.6 \leqslant R_{\mathrm{p}} \leqslant 1.75\,R_{\mathrm{Jup}}$.
    C. $R_{\mathrm{p}} \geqslant 1.75\,R_{\mathrm{Jup}}$.

(ii) Exoplanet diagnostic η_{p}.

    A. $0.5 \geqslant \eta_{\mathrm{p}} \geqslant 1.5$.
    B. $\eta_{\mathrm{p}} < 0.5$.
    C. $\eta_{\mathrm{p}} \geqslant 1.5$.

(iii) Blending.

    A. No other objects within aperture.
    B. One or two other objects less than 5 mag fainter than target within aperture.
    C. More than two objects less than 5 mag fainter than target within aperture.
    D. Brighter objects within the aperture.

Each candidate was then assessed in turn, taking into account all available data, and a final short list of high-priority candidates was produced. In the next section we summarize the results for stars in the RA range 18–21 h.

It can be seen from this discussion that some selection cuts are repeated during subsequent stages using increasingly stringent thresholds. For instance, HUNTSMAN executes an automatic cut of objects with $S_{\mathrm{red}} < 5.0$, while at stage 3, a further cut is made at $S_{\mathrm{red}} < 8.0$. In exploring the first large-scale transit hunting results from SW, we took a cautious approach in order to investigate the most effective selection criteria. Not wanting the algorithm to dismiss interesting objects before human interpretation, the initial thresholds were set low, systematically rising for successive stages of evaluation. Needless to say, lessons learned from this season's work will enable us to streamline the procedure in future.

4 RESULTS

The HUNTSMAN algorithm flagged 11 626 objects for attention. Stage 2 visual inspection concluded that 775 of these were of genuine interest. The stage 3 selection requirements detailed in Section 3.3 sifted this list down to 77 stars, the details of which are presented in Table 2.

The visual light curve assessment of each star is quantified by a four-digit code in column 11. At this stage, the list contained 19 borderline candidates, many of which are likely low-mass binaries. As these objects are of independent interest, we have included their full parameters in Tables 2 and 3, marked by †, although these objects

Table 2. Initial list of candidates after stage 3. Borderline candidates are marked with [†] and are listed for information.

Identifier 1SWASP...	V_{SW} (mag)	Period (d)	Duration (h)	δ (mag)	N_t	S_{red}	$\Delta\chi^2$	S/N$_{ellip}$	$\Delta\chi^2/\Delta\chi^2_-$	Code
[†]J175919.79+353935.1	11.824	4.846 186	4.272	0.026	6	9.264	338.197	0.605	5.327	2223
[†]J180103.13+511557.1	9.988	4.785 081	3.672	0.0145	8	11.215	928.888	2.401	3.467	2423
J180304.96+264805.4	11.782	2.364 723	5.136	0.0254	20	13.453	1 454.973	4.145	9.616	3211
J180726.64+224227.9	12.568	2.121 623	5.256	0.0173	21	9.548	375.908	4.150	3.302	3314
[†]J181129.19+235412.4	12.884	4.234 895	8.568	0.0578	16	11.584	2 580.622	1.699	9.145	1314
J181317.03+305356.0	**12.046**	**4.498 677**	**1.92**	**0.0194**	**13**	**14.446**	**540.914**	**4.992**	**6.704**	**1134**
J181454.99+391146.0	**12.796**	**1.102 625**	**1.56**	**0.0235**	**25**	**13.297**	**219.564**	**0.659**	**5.134**	**1212**
J181958.25+492329.9	**10.6**	**2.368 548**	**2.424**	**0.0061**	**16**	**10.759**	**145.924**	**0.241**	**2.902**	**3111**
J182127.09+200011.7	11.449	2.647 752	4.248	0.0366	18	16.824	2 831.871	2.789	15.396	1111
J182131.07+483735.5	12.164	1.809 191	2.832	0.0167	16	9.781	470.931	2.314	4.140	3211
J182333.22+222801.2	12.788	1.821 008	3.432	0.0421	18	17.315	983.6475	8.064	12.2324	1211
[†]J182339.64+210805.5	12.794	1.585 846	2.088	0.0245	22	10.374	306.613	6.991	2.312	1314
J182346.12+434241.3	11.771	2.969 366	3.384	0.0295	11	19.982	444.963	0.895	11.656	1124
J182620.36+475902.8	**11.584**	**3.04 365**	**4.032**	**0.0628**	**13**	**24.415**	**10 754.299**	**4.225**	**11.474**	**1112**
[†]J182626.38+374954.8	11.614	4.698 312	4.944	0.0157	8	13.104	317.828	1.643	6.417	2213
J182916.00+235724.8	12.043	4.465 326	1.752	0.0373	7	12.356	578.442	3.163	11.565	2224
J182924.67+232200.2	**11.331**	**3.678 186**	**2.952**	**0.0173**	**10**	**14.248**	**244.980**	**2.174**	**2.639**	**3123**
[†]J182927.04+233217.1	10.8	4.903 747	4.704	0.0063	9	8.214	146.459	1.954	2.299	3214
[†]J183043.97+230526.1	9.31	3.680 977	4.296	0.0098	9	11.139	628.645	3.278	4.027	2311
J183104.01+323942.7	**11.027**	**2.378 781**	**1.776**	**0.0089**	**15**	**11.013**	**256.230**	**2.065**	**4.873**	**2111**
J183104.12+243739.3	12.789	1.492 383	1.92	0.0197	20	10.218	188.009	4.411	2.836	1314
J183431.62+353941.4	**10.485**	**1.846 796**	**2.28**	**0.0127**	**17**	**12.111**	**787.959**	**0.691**	**3.635**	**1111**
[†]J183517.51+390316.2	9.823	4.073 428	5.16	0.012	8	9.282	1 320.766	5.377	2.225	1123
J183723.62+373721.9	11.851	3.300 887	4.32	0.0251	13	13.599	841.3629	8.779	10.1919	1213
J183805.57+423432.3	**12.641**	**3.515 957**	**4.104**	**0.0197**	**9**	**8.815**	**127.097**	**0.999**	**3.693**	**3131**
J184119.02+403008.4	**12.157**	**3.734 014**	**4.224**	**0.0148**	**11**	**9.449**	**198.451**	**0.502**	**2.720**	**3133**
J184303.62+462656.4	**11.935**	**3.338 103**	**4.08**	**0.0265**	**11**	**12.248**	**1 065.843**	**1.867**	**9.098**	**4124**
J202820.25+094651.0	11.108	2.146 933	4.776	0.0085	16	12.533	294.491	3.910	5.344	2111
J202824.02+192310.2	**12.16**	**1.257 835**	**2.424**	**0.0222**	**23**	**13.111**	**589.550**	**3.355**	**7.095**	**1111**
[†]J202907.09+171631.7	12.786	4.117 398	4.968	0.0309	11	9.996	450.143	1.126	3.844	2223
J203054.12+062546.4	**11.98**	**2.152 102**	**1.296**	**0.0168**	**11**	**9.463**	**217.184**	**5.522**	**3.262**	**1111**
[†]J203229.10+132820.9	12.471	4.632 829	4.608	0.047	9	12.773	1 385.902	2.670	11.318	2213
J203247.55+182805.3	12.157	2.522 688	7.776	0.0118	22	11.579	308.408	0.875	5.324	3113
J203314.77+092823.4	**11.78**	**1.753 056**	**3.048**	**0.0316**	**18**	**14.221**	**2 154.619**	**7.012**	**8.927**	**1111**
J203315.84+092854.2	**11.943**	**1.752 371**	**2.784**	**0.0413**	**16**	**13.545**	**2 796.5991**	**9.663**	**11.4699**	**1211**
J203543.98+072641.1	10.094	1.85 463	2.76	0.0195	13	16.884	3 354.689	1.083	10.542	1112
J203704.92+191525.1	**11.301**	**1.68 011**	**1.416**	**0.0095**	**16**	**9.344**	**245.231**	**3.226**	**2.826**	**3111**
J203717.02+114253.5	11.327	3.118 049	2.496	0.0274	8	12.11	2 792.375	3.870	21.267	1111
J203906.39+171345.9	**9.716**	**1.348 858**	**1.968**	**0.0173**	**18**	**17.059**	**2 934.2539**	**8.365**	**47.1445**	**1124**
[†]J203932.30+162451.1	10.904	1.520 504	8.976	0.02	39	14.359	10 012.064	0.966	2.936	2311
J204125.28+163911.8	**11.243**	**1.221 506**	**2.88**	**0.008**	**28**	**11.48**	**518.131**	**2.703**	**3.151**	**3111**
[†]J204142.31+052007.5	12.422	3.216 912	4.776	0.0279	8	10.462	317.078	0.533	7.574	2232
J204142.49+075051.5	**12.082**	**1.381 342**	**1.968**	**0.0096**	**19**	**11.739**	**165.756**	**1.413**	**7.403**	**3114**
J204211.19+240145.1	11.588	1.792 911	2.424	0.0518	10	14.079	1074.758	6.535	2.917	4134
J204323.83+263818.7	**11.561**	**1.419 959**	**1.2**	**0.0369**	**10**	**18.496**	**179.712**	**0.971**	**2.440**	**1224**
[†]J204328.95+054823.1	12.616	3.939 179	2.328	0.0617	10	16.96	1989.211	5.293	17.029	1322
(J204456.57+182136.0	12.596	2.71 611	4.584	0.0202	16	12.164	525.040	1.287	14.612	3214)[a]
J204617.02+085412.0	**12.28**	**1.947 141**	**2.184**	**0.0095**	**14**	**9.436**	**92.943**	**0.647**	**2.163**	**3112**
J204712.42+202544.5	**12.386**	**2.61 264**	**2.064**	**0.0275**	**10**	**13.103**	**355.276**	**3.327**	**6.693**	**2211**
J204745.08+103347.9	**11.648**	**3.235 407**	**3.648**	**0.0289**	**8**	**16.376**	**1336.114**	**5.186**	**16.348**	**1112**
[†]J204905.55+110000.4	12.891	1.371 571	1.584	0.023	20	12.8	244.376	4.343	4.619	1311
J205027.33+064022.9	**10.164**	**1.229 345**	**3.192**	**0.0096**	**20**	**13.641**	**1198.006**	**6.691**	**5.830**	**3111**
[†]J205218.75+182330.0	11.991	2.197 814	3.48	0.0441	16	19.038	3378.642	3.256	22.912	1131
J205223.03+151046.8	11.493	1.454 887	2.4	0.0301	23	19.47	3389.000	2.060	21.470	1114
J205302.40+201748.3	10.853	4.931 719	8.88	0.0084	9	8.327	360.930	0.093	2.553	3123
J205308.03+192152.7	**11.13**	**1.676 449**	**2.736**	**0.0068**	**23**	**10.406**	**213.332**	**0.668**	**3.508**	**2111**
J205438.05+105040.7	11.428	2.623 442	2.664	0.0405	11	16.117	3278.368	4.645	8.251	1114
J210009.75+193107.1	**10.422**	**3.054 875**	**2.424**	**0.0082**	**9**	**8.877**	**303.455**	**1.646**	**2.612**	**3113**
[†]J210130.24+190021.7	12.14	2.683 587	1.584	0.0697	12	23.253	1860.082	5.557	31.460	1311
J210151.43+072326.7	**12.476**	**2.220 785**	**2.472**	**0.0138**	**15**	**8.764**	**108.956**	**0.948**	**2.396**	**3213**
[†]J210231.79+101014.5	12.635	1.506 187	1.608	0.0296	16	14.97	258.766	6.760	2.971	1332

Table 2 – *continued*

Identifier 1SWASP...	V_{SW} (mag)	Period (d)	Duration (h)	δ (mag)	N_t	S_{red}	$\Delta\chi^2$	S/N_{ellip}	$\Delta\chi^2/\Delta\chi^2_-$	Code
J210318.01+080117.8	**11.909**	**1.223 824**	**1.92**	**0.0167**	**24**	**12.784**	**466.284**	**0.248**	**4.999**	**1111**
†J210335.82+125637.6	12.387	1.447 543	2.856	0.0146	24	9.082	268.208	1.208	4.420	2213
J210352.56+083258.9	**11.636**	**3.89 368**	**3.504**	**0.0227**	**11**	**13.38**	**953.011**	**7.066**	**11.909**	**1112**
J210909.05+184950.9	**9.912**	**2.91 879**	**2.664**	**0.0083**	**13**	**9.718**	**801.126**	**0.121**	**3.041**	**3112**
J210912.02+073843.3	**11.262**	**1.36 983**	**2.28**	**0.0213**	**22**	**16.035**	**1594.4681**	**12.508**	**20.6406**	**1111**
J211127.41+182653.3	12.291	4.216 933	3.168	0.0464	8	20.186	1043.324	0.775	25.743	2211
J211417.15+112741.0	11.246	2.519 934	2.784	0.0336	11	10.555	2902.904	1.290	3.334	3214
J211448.98+203557.1	12.453	4.864 666	4.632	0.0525	8	13.794	1939.578	4.542	16.558	1212
J211608.42+163220.3	**11.308**	**3.468 244**	**1.992**	**0.0131**	**10**	**13.461**	**228.680**	**0.781**	**5.584**	**1111**
J211645.22+192136.8	**9.432**	**1.466 001**	**1.68**	**0.012**	**16**	**12.273**	**1379.556**	**2.033**	**3.516**	**2124**
J211817.92+182659.9	12.395	4.419 854	3.36	0.0274	9	12.149	716.481	1.194	9.733	3214
J212532.55+082904.4	**11.343**	**3.125 014**	**2.688**	**0.0267**	**9**	**14.313**	**1013.935**	**1.980**	**7.591**	**1212**
J212749.35+190246.0	12.317	4.870 738	3.408	0.0438	10	10.158	1332.879	1.191	2.215	2224
†J212815.28+082933.7	10.165	4.91 815	5.592	0.0083	9	8.493	374.959	0.644	2.249	3414
J212843.62+160806.2	**11.453**	**1.375 647**	**2.64**	**0.0159**	**25**	**15.572**	**1288.665**	**8.841**	**9.5499**	**1111**
J212855.03+075753.5	**12.241**	**4.688 048**	**1.92**	**0.0297**	**5**	**9.54**	**188.137**	**0.953**	**2.503**	**3213**

^{a}Parenthesis around an object indicates that spectroscopic data are discussed in Section 5.

were not carried through to the final short-listing as the present paper deals with planetary candidates only.

The remaining 58 objects surviving to stage 4 could be grouped into three broad classes. 24 stars received the best grades (between '1111' and '2222'), indicating a clear, credible transit signal in a flat, well-sampled light curve. 17 objects were flagged as displaying a credible transit signal, but on a period not correctly identified. A further 17 candidates were found to show plausible transits signals and were only downgraded on the grounds of low S/N.

At this stage we attempted to eliminate astrophysical false positives by considering the catalogue information available, estimating the companion radius and corresponding value of η_p and assessing the degree of blending in the field.

Table 3 gives the full set of parameters for these candidates. Each candidate was then evaluated on its merits, including a visual examination of both folded and unfolded light curves. Where relevant, target light curves were refolded on the periods of the alternative peaks from the periodogram. In a small number of cases, this showed that the true period fell outside HUNTSMAN's search range of 0.9–5 d. We then applied the algorithm developed by Schwarzenberg-Czerny (1989, 1999, hereafter S-C) to determine the correct period.

Evaluating all the information available for all candidates highlighted 35 objects of particular interest at the stage 4; the remaining objects being rejected as likely stellar binaries, some blended. These are printed in bold in Tables 2 and 3 and their folded light curves and $\Delta\chi^2$ periodograms are presented in Figs 3–7. We discuss these objects individually below, and indicate particularly strong planetary candidates. However, all of these objects deserve follow-up observations as 'false alarms' from a transit survey include interesting low-mass binaries.

4.1 1SWASP J181317.03+305356.0

This object displayed a distinct, if noisy, dip when folded on its original period of 4.499 d but this resulted in gaps in the phase coverage. The transit is still visible when the data are folded on a period of 2.248 d but this time the light curve is more smoothly sampled and flat out of transit to visual inspection. The new parameters imply a Jovian-sized companion object ($R_p = 1.05 R_{Jup}$) supported by a reasonable $\eta_p = 0.71$, but while the target is the brightest object

in its field it has sufficient nearby faint stars for blending to be a possibility. More observations are required for this object.

4.2 1SWASP J181454.99+391146.0

The faintness of this object (12.796 mag) accounts for the degree of noise in the light curve, but the transit is still visible. The noise makes it difficult to judge the flatness out of transit, though the S/N_{ellip} is 0.659. The period is close to the 1-d alias at 1.10 d, but this is derived from a clear strong peak in $\Delta\chi^2$. Otherwise, the amplitude and the transit duration are reasonable, supported by an $\eta_p = 0.92$. The primary star appears to be late type, implying a relatively small companion ($0.89 R_{Jup}$). However, this object lies in a fairly crowded field, so it may be a blended stellar binary.

4.3 1SWASP J181958.25+492329.9

The brightness of this 10.6 mag object allows us to detect transits only ~6 mmag deep in this flat light curve. The period was confirmed independently with the S-C algorithm and transit signatures identified by visual inspection of the unfolded light curve. The host star has a solar spectral type so the estimated companion radius is very low: $0.69 R_{Jup}$, supported by an η_p close to 1. This makes it an exciting candidate for follow-up despite the serious crowding in this field. However, further observations are required to eliminate the possibility of a blended eclipsing binary.

4.4 1SWASP J182620.36+475902.8

The folded light curve clearly shows a fairly deep, wide, 'V'-shaped dip (which might indicate a stellar binary) but no obvious ellipsoidal variations. The period is 3.04 d, close to a multiple of the 1-d alias, but the signal is clear with a credible number of transits observed. The object is unblended and has an estimated companion radius of $1.6 R_{Jup}$; however the η_p of 1.49 would support the stellar binary hypothesis.

4.5 1SWASP J182924.67+232200.2

We handle this object with caution because the transit signature is unclear for the partially owing to its period (3.68 d) and also to the

intrinsic scatter in the light curve. Nevertheless, transit-like dips were identified from visual inspection of the unfolded light curve. No other variability is evident. The companion radius is credible for a planet at $1.26\,R_{\rm Jup}$ supported by $\eta_{\rm p} = 0.88$. This star is significantly brighter than any other object within $\sim$3 arcmin although blending cannot be ruled out. We recommend obtaining more data on this object to confirm the transit-like signal.

4.6 1SWASP J183104.01+323942.7

The low amplitude (0.0089 mag) and short duration (1.8 h) of this event would have made it difficult to detect in a fainter star. Our light curve shows little out-of-transit variation and a clear, credible period. The predicted radius of $0.97\,R_{\rm Jup}$ is supported by a slightly low but acceptable value of $\eta_{\rm p} = 0.61$. As this candidate lies in an uncrowded field it is a strong planetary candidate.

4.7 1SWASP J183431.62+353941.4

The classic, flat-bottomed transit signature is clear in the folded light curve of this bright (10.5 mag) star, which shows no other signs of variability and a reasonable if quite short period. The companion radius of $1.3\,R_{\rm Jup}$ is within the expected range for a hot Jupiter, and an $\eta_{\rm p}$ of 0.78 makes it believable. The high degree of blending around this candidate raises a warning flag for an otherwise strong candidate.

4.8 1SWASP J183805.57+423432.3

This folded light curve shows a degree of clumping because the period of $\sim$3.5 d requires a longer time-base of observations to cover the full phase range. Dips are clearly visible in the unfolded data although the $V \sim 12.6$ mag means there is a high degree of intrinsic

Table 3. Candidate list after stage 4. $N_{\rm bri,faint}$ gives the number of USNO-B1.0 objects listed within 48 arcsec of the target that are brighter or <5 mag fainter, respectively. Spectral types marked with an asterisk were estimated from the 2MASS $J - H$ index in cases where the $V_{\rm SW} - K$ index was at the extremity of the range, and unreliable. Borderline candidates are marked with † and are listed for information.

Identifier 1SWASP...	Period (d)	Duration (h)	δ (mag)	$V_{\rm SW} - K$	$J - H$	Spectral type	R_* (R$_\odot$)	$R_{\rm p}$ (R$_{\rm Jup}$)	$\eta_{\rm p}$	$N_{\rm bri}$	$N_{\rm faint}$	R	Code Eta	Blend
†J175919.79+353935.1	4.846 186	4.272	0.026	3.51	0.61	M0	0.64	0.88	1.58	0	2	A	C	B
†J180103.13+511557.1	4.785 081	3.672	0.0145	2.46	0.48	K4	0.73	0.75	1.3	0	1	B	A	B
J180304.96+264805.4	2.364 723	5.136	0.0254	2.52	0.53	K4	0.72	0.98	2.26	0	6	A	C	C
J180726.64+224227.9	4.246 971	4.752	0.0205	1.91	0.29	G9	0.87	1.06	1.56	0	2	A	C	B
†J181129.19+235412.4	4.234 895	8.568	0.0578	1.91	0.48	G9	0.87	1.78	2.61	0	2	C	C	B
J181317.03+305356.0	**2.248 420**	**1.896**	**0.0145**	**1.6**	**0.28**	**G3**	**1.02**	**1.05**	**0.71**	**0**	**2**	**A**	**A**	**B**
J181454.99+391146.0	**1.102 625**	**1.56**	**0.0235**	**2.89**	**0.74**	**K5**	**0.68**	**0.89**	**0.92**	**0**	**10**	**A**	**A**	**C**
J181958.25+492329.9	**2.368 548**	**2.424**	**0.0061**	**1.57**	**0.26**	**G2**	**1.04**	**0.69**	**0.92**	**0**	**2**	**A**	**A**	**B**
J182127.09+200011.7	2.647 752	4.248	0.0366	1.26	0.18	F7	1.25	2.04	1.27	0	6	C	A	C
J182131.07+483735.5	1.809 191	2.832	0.0167	0.56	0.26	A7-F0	1.79	1.97	0.82	0	3	C	C	C
J182333.22+222801.2	1.821 008	3.432	0.0421	1.59	0.21	G3	1.03	1.8	1.29	0	2	C	A	B
†J182339.64+210805.5	1.585 846	2.088	0.0245	1.16	0.28	F6	1.32	1.76	0.74	0	13	C	A	C
J182346.12+434241.3	11.87 746	6.841	0.065	1.26	0.19	F7	1.25	2.72	1.19	0	1	C	A	B
J182620.36+475902.8	**3.04 365**	**4.032**	**0.0628**	**2.35**	**0.45**	**K3**	**0.75**	**1.6**	**1.49**	**0**	**0**	**B**	**A**	**A**
†J182626.38+374954.8	4.698 312	4.944	0.0157	1.26	0.25	F7	1.25	1.34	1.29	0	6	A	A	C
J182916.00+235724.8	8.901 122	4.168	0.038	1.48	0.34	G0	1.1	1.83	0.9	0	6	C	A	C
J182924.67+232200.2	**3.678 186**	**2.952**	**0.0173**	**1.45**	**0.21**	**G0**	**1.12**	**1.26**	**0.88**	**0**	**3**	**A**	**A**	**C**
†J182927.04+233217.1	4.903 747	4.704	0.0063	2.5	0.52	K4	0.73	0.49	1.71	0	5	A	C	C
†J183043.97+230526.1	3.680 977	4.296	0.0098	1.68	0.26	G5	0.98	0.83	1.43	0	2	A	A	B
J183104.01+323942.7	**2.378 781**	**1.776**	**0.0089**	**1.33**	**0.21**	**F8**	**1.2**	**0.97**	**0.61**	**0**	**2**	**A**	**A**	**B**
J183104.12+243739.3	0.746 192	3.836	0.0197	1.47	0.23	G0	1.1	1.32	1.96	0	6	A	C	C
J183431.62+353941.4	**1.846 796**	**2.28**	**0.0127**	**1.12**	**0.2**	**F5**	**1.35**	**1.3**	**0.78**	**0**	**3**	**A**	**A**	**C**
†J183517.51+390316.2	4.073 428	5.16	0.012	2.71	0.49	K5	0.7	0.65	2	0	7	A	C	C
J183723.62+373721.9	3.300 887	4.32	0.0251	2.69	0.51	K5	0.7	0.95	1.73	0	4	A	C	C
J183805.57+423432.3	**3.515 957**	**4.104**	**0.0197**	**2.51**	**0.55**	**K4**	**0.72**	**0.86**	**1.6**	**0**	**4**	**A**	**C**	**C**
J184119.02+403008.4	**3.734 014**	**4.224**	**0.0148**	**1.86**	**0.29**	**G8**	**0.89**	**0.92**	**1.45**	**0**	**1**	**A**	**A**	**B**
J184303.62+462656.4	**10.07 384**	**7.253**	**0.037**	**2.3**	**0.55**	**K3**	**0.76**	**1.25**	**1.86**	**0**	**3**	**A**	**C**	**C**
J202820.25+094651.0	2.146 933	4.776	0.0085	2.37	0.48	K3	0.75	0.59	2.23	0	2	A	C	B
J202824.02+192310.2	**1.257 835**	**2.424**	**0.0222**	**1.2**	**0.2**	**F6**	**1.29**	**1.64**	**0.94**	**0**	**8**	**B**	**A**	**C**
†J202907.09+171631.7	4.117 398	4.968	0.0309	1.61	0.37	G3	1.02	1.53	1.46	0	13	A	A	C
J203054.12+062546.4	**2.152 102**	**1.296**	**0.0168**	**2.35**	**0.41**	**K3**	**0.75**	**0.83**	**0.59**	**0**	**3**	**A**	**A**	**C**
†J203229.10+132820.9	4.632 829	4.608	0.047	2.35	0.61	K3	0.75	1.39	1.51	0	15	A	C	C
J203247.55+182805.3	2.522 688	7.776	0.0118	1.42	0.27	F9	1.14	1.06	2.66	0	10	A	C	C
J203314.77+092823.4	**1.753 056**	**3.048**	**0.0316**	**3.87**	**0.77**	**M0**	**0.62**	**0.94**	**1.59**	**0**	**2**	**A**	**C**	**B**
J203315.84+092854.2	**1.752 371**	**2.784**	**0.0413**	**−0.46**	**0.198**	**F2-F5***	**1.46**	**2.53**	**0.87**	**1**	**12**	**C**	**A**	**C**
J203543.98+072641.1	1.85 463	2.76	0.0195	0.99	0.24	F3	1.43	1.7	0.9	0	3	B	A	C
J203704.92+191525.1	**1.68 011**	**1.416**	**0.0095**	**1.37**	**0.27**	**F9**	**1.17**	**0.97**	**0.55**	**0**	**2**	**A**	**A**	**B**
J203717.02+114253.5	3.118 049	2.496	0.0274	1.31	0.25	F8	1.21	1.71	0.74	0	1	B	A	B
J203906.39+171345.9	**2.696 631**	**2.184**	**0.0217**	**1.33**	**0.22**	**F8**	**1.2**	**1.35**	**0.79**	**0**	**2**	**A**	**A**	**B**
†J203932.30+162451.1	1.520 504	8.976	0.02	3.35	0.62	K7	0.65	0.78	4.92	0	2	A	C	B
J204125.28+163911.8	**1.221 506**	**2.88**	**0.008**	**2.77**	**0.54**	**K5**	**0.69**	**0.53**	**1.71**	**0**	**4**	**A**	**C**	**C**
†J204142.31+052007.5	3.216 912	4.776	0.0279	2.05	0.38	K0	0.82	1.17	1.75	0	5	A	C	C
J204142.49+075051.5	**2.763 125**	**2.328**	**0.0102**	**2.86**	**0.59**	**K5**	**0.69**	**0.59**	**1.04**	**0**	**4**	**A**	**A**	**C**

Table 3 – *continued*

Identifier 1SWASP...	Period (d)	Duration (h)	δ (mag)	$V_{SW} - K$	$J - H$	Spectral type	R_* ($R_\odot$)	R_p (R_{Jup})	η_p	N_{bri}	N_{faint}		Code	
J204211.19+240145.1	3.362 228	2.664	0.0544	1.65	0.19	G4	1.0	1.99	0.81	0	2	C	C	B
J204323.83+263818.7	**1.421 123**	**1.32**	**0.0366**	**2.1**	**0.32**	**K1**	**0.81**	**1.32**	**0.63**	**0**	**2**	**A**	**A**	**B**
†J204328.95+054823.1	3.939 179	2.328	0.0617	1.69	0.25	G5	0.97	2.06	0.68	0	2	C	A	B
(J204456.57+182136.0	8.147 196	7.821	0.044	1.61	0.24	G3	1.02	1.83	1.79	0	2	C	C	B)[a]
J204617.02+085412.0	**1.947 141**	**2.184**	**0.0095**	**1.48**	**0.25**	**G0**	**1.1**	**0.91**	**0.84**	**0**	**5**	**A**	**A**	**C**
J204712.42+202544.5	**2.61 264**	**2.064**	**0.0275**	**3.01**	**0.58**	**K5***	**0.67**	**0.95**	**0.91**	**0**	**8**	**A**	**A**	**C**
J204745.08+103347.9	**3.235 407**	**3.648**	**0.0289**	**2.79**	**0.63**	**K7***	**0.69**	**1.00**	**1.47**	**0**	**2**	**A**	**A**	**B**
†J204905.55+110000.4	1.371 571	1.584	0.023	1.07	0.24	F5	1.38	1.79	0.57	0	7	C	A	C
J205027.33+064022.9	**1.229 345**	**3.192**	**0.0096**	**1.47**	**0.24**	**G0**	**1.1**	**0.92**	**1.43**	**0**	**2**	**A**	**A**	**B**
†J205218.75+182330.0	2.197 814	3.48	0.0441	1.45	0.2	G0	1.12	2.01	1.17	0	4	C	A	C
J205223.03+151046.8	2.910 170	2.400	0.0409	1.5	0.2	G1	1.08	1.86	0.75	0	0	C	A	A
J205302.40+201748.3	4.931 719	8.88	0.0084	1.58	0.33	G2	1.03	0.81	2.61	0	1	A	C	B
J205308.03+192152.7	**1.676 449**	**2.736**	**0.0068**	**1.27**	**0.21**	**F7**	**1.24**	**0.87**	**1.04**	**0**	**5**	**A**	**A**	**C**
J205438.05+105040.7	4.198 031	3.048	0.0468	1.42	0.19	F9	1.14	2.10	0.81	0	0	C	A	A
J210009.75+193107.1	**3.054 875**	**2.424**	**0.0082**	**1.08**	**0.11**	**F5**	**1.38**	**1.07**	**0.71**	**0**	**1**	**A**	**A**	**B**
†J210130.24+190021.7	2.683 466	1.608	0.0709	1.9	0.34	G9	0.88	2	0.56	0	3	C	A	C
J210151.43+072326.7	**2.220 785**	**2.472**	**0.0138**	**1.79**	**0.33**	**G7**	**0.92**	**0.92**	**0.99**	**0**	**3**	**A**	**A**	**C**
†J210231.79+101014.5	1.506 187	1.608	0.0296	1.79	0.35	G7	0.92	1.35	0.71	0	6	A	A	C
J210318.01+080117.8	**1.223 824**	**1.92**	**0.0167**	**1.79**	**0.31**	**G7**	**0.92**	**1.01**	**0.93**	**0**	**1**	**A**	**A**	**B**
†J210335.82+125637.6	1.447 543	2.856	0.0146	1.27	0.18	F7	1.24	1.28	1.11	0	2	A	A	B
J210352.56+083258.9	**3.89 368**	**3.504**	**0.0227**	**1.25**	**0.2**	**F7**	**1.25**	**1.61**	**0.95**	**0**	**3**	**B**	**A**	**C**
J210909.05+184950.9	**2.91 879**	**2.664**	**0.0083**	**0.86**	**0.07**	**F1**	**1.51**	**1.17**	**0.75**	**0**	**3**	**A**	**A**	**C**
J210912.02+073843.3	**1.36 983**	**2.28**	**0.0213**	**1.3**	**0.21**	**F8**	**1.22**	**1.52**	**0.89**	**0**	**2**	**A**	**A**	**B**
J211127.41+182653.3	4.216 933	3.168	0.0464	1.44	0.19	G0	1.12	2.06	0.85	0	5	C	A	C
J211417.15+112741.0	6.579 094	8.23	0.0336	1.6	0.35	G3	1.02	1.6	2.06	0	3	B	C	C
J211448.98+203557.1[b]	4.864 623	4.656	0.0530	1.63	0.25	G3	1.01	1.98	1.25	0	4	C	A	C
J211448.98+203557.1[b]	4.864 666	4.632	0.0525	1.63	0.25	G3	1.01	1.98	1.25	0	4	C	A	C
J211608.42+163220.3	**3.468 244**	**1.992**	**0.0131**	**1.31**	**0.21**	**F8**	**1.21**	**1.18**	**0.59**	**0**	**0**	**A**	**A**	**A**
J211645.22+192136.8	**4.400 381**	**2.640**	**0.0135**	**1.27**	**0.16**	**F7**	**1.24**	**1.23**	**0.71**	**0**	**0**	**A**	**A**	**A**
J211817.92+182659.9	7.715 382	8.888	0.0357	1.04	0.3	F4	1.4	2.45	0.4	0	7	C	B	C
J212532.55+082904.4	**3.125 014**	**2.688**	**0.0267**	**1.43**	**0.23**	**F9**	**1.13**	**1.58**	**0.82**	**0**	**0**	**A**	**A**	**A**
J212749.35+190246.0	7.810 082	8.4	0.10	2.08	0.34	K1	0.82	2.21	2.05	0	1	C	C	B
†J212815.28+082933.7	4.91 815	5.592	0.0083	1.27	0.23	F7	1.24	0.96	1.48	0	3	A	A	C
J212843.62+160806.2	**1.375 647**	**2.64**	**0.0159**	**2.59**	**0.53**	**K5***	**0.71**	**0.76**	**1.44**	**0**	**3**	**A**	**A**	**C**
J212855.03+075753.5	**4.688 048**	**1.92**	**0.0297**	**1.8**	**0.36**	**G7**	**0.92**	**1.35**	**0.58**	**0**	**2**	**A**	**A**	**B**

[a]Parenthesis around an object indicates that spectroscopic data are discussed in Section 5.

[b]1SWASP J211448.98+203557.1 was identified in two fields, SW2114+1628 and SW2115+2351 and independent results are given for each.

scatter in the data. However, the star lies in a relatively uncrowded field and the nearest companions are $\gtrsim 10$ arcmin away. The late-type host star leads us to infer a small companion radius of $0.86 R_{Jup}$. Although this is tempered by an η_p of 1.6, this object remains a candidate.

4.9 1SWASP J184119.02+403008.4

The transit signature in this folded light curve is unclear for the same reasons given for 1SWASP J183805.57+423432.3. As above, the validity of the measured signal was confirmed by visual inspection of the unfolded data. No other variation is evident in the light curve. The predicted companion radius of $0.92 R_{Jup}$ is tempered by a slightly elevated $\eta_p = 1.45$, but is the brightest object in an uncrowded field.

4.10 1SWASP J184303.62+462656.4

The original light curve showed a 'V'-shaped dip at phase 0.0 with additional points around phase −0.45, which gave the appearance that the correct period was not identified. The gaps in the light curve indicate that the true period lies close to an alias making it difficult to determine. This is supported by investigation with

the S-C algorithm, which suggested a period around 10 d; the light curve in Fig. 4(b) is shown folded on the strongest peak found by HUNTSMAN. The predicted companion radius given these parameters is only $1.25 R_{Jup}$, although the eclipse durations are longer than those expected for a planetary transit ($\eta_p = 1.86$). This object could be a low-mass binary and although it suffers from blending, we recommend that it continue to be observed.

4.11 1SWASP J202824.02+192310.2

This object displays transits of credible width and depth in an otherwise flat, if noisy, light curve. The host star colour implies a radius of $1.29 R_\odot$ and a fairly large companion object at $1.64 R_{Jup}$ ($\eta_p = 0.94$). However, light from a number of nearby stars will have contaminated the photometry, so this could be a stellar binary.

4.12 1SWASP J203054.12+062546.4

The data for this target show a brief but quite well defined signal in an otherwise flat, if noisy, light curve. The period and amplitude are believable for a planetary companion of $0.83 R_{Jup}$ with a low but

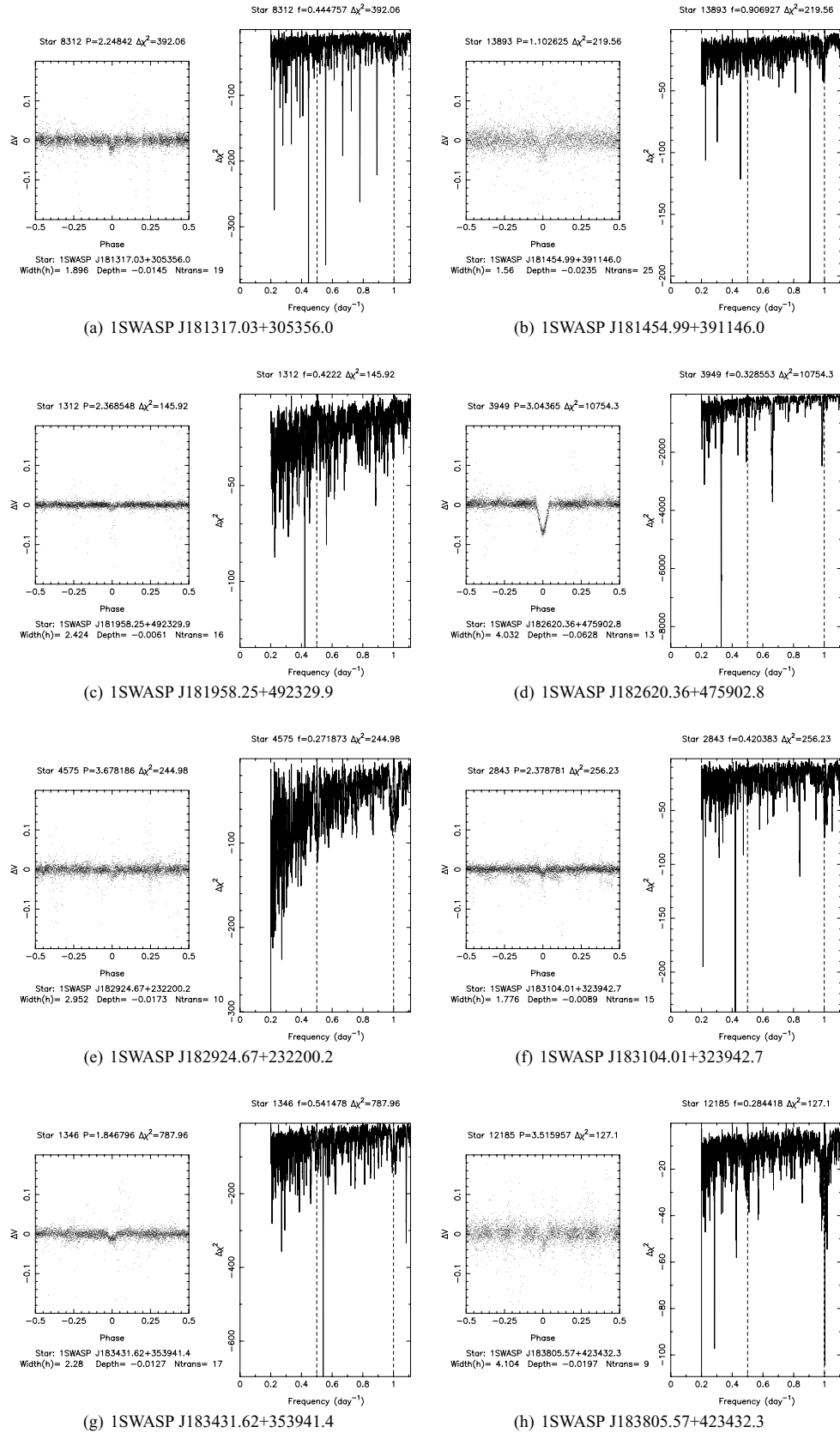(a) 1SWASP J181317.03+305356.0

(b) 1SWASP J181454.99+391146.0

(c) 1SWASP J181958.25+492329.9

(d) 1SWASP J182620.36+475902.8

(e) 1SWASP J182924.67+232200.2

(f) 1SWASP J183104.01+323942.7

(g) 1SWASP J183431.62+353941.4

(h) 1SWASP J183805.57+423432.3

Figure 3. The light curves of the selected transit candidates, folded on the measured period.

(a) 1SWASP J184119.02+403008.4

(b) 1SWASP J184303.62+462656.4

(c) 1SWASP J202824.02+192310.2

(d) 1SWASP J203054.12+062546.4

(e) 1SWASP J203314.77+092823.4

(f) 1SWASP J203315.84+092854.2

(g) 1SWASP J203704.92+191525.1

(h) 1SWASP J203906.39+171345.9
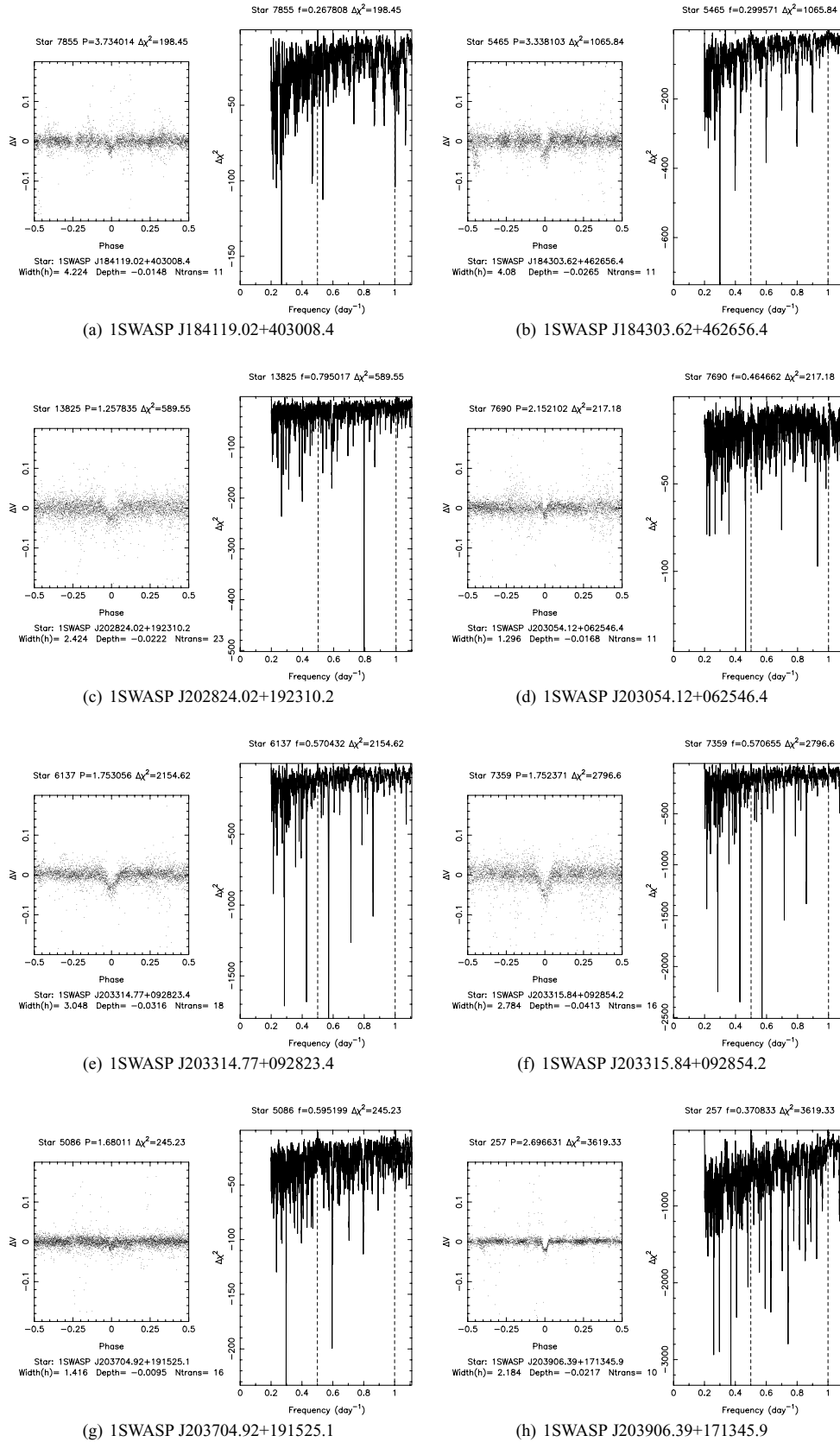
Figure 4. The light curves of the selected transit candidates, folded on the measured period.

(a) 1SWASP J204125.28+163911.8

(b) 1SWASP J204142.49+075051.5

(c) 1SWASP J204323.83+263818.7

(d) 1SWASP J204617.02+085412.0

(e) 1SWASP J204712.42+202544.5

(f) 1SWASP J204745.08+103347.9

(g) 1SWASP J205027.33+064022.9

(h) 1SWASP J205308.03+192152.7
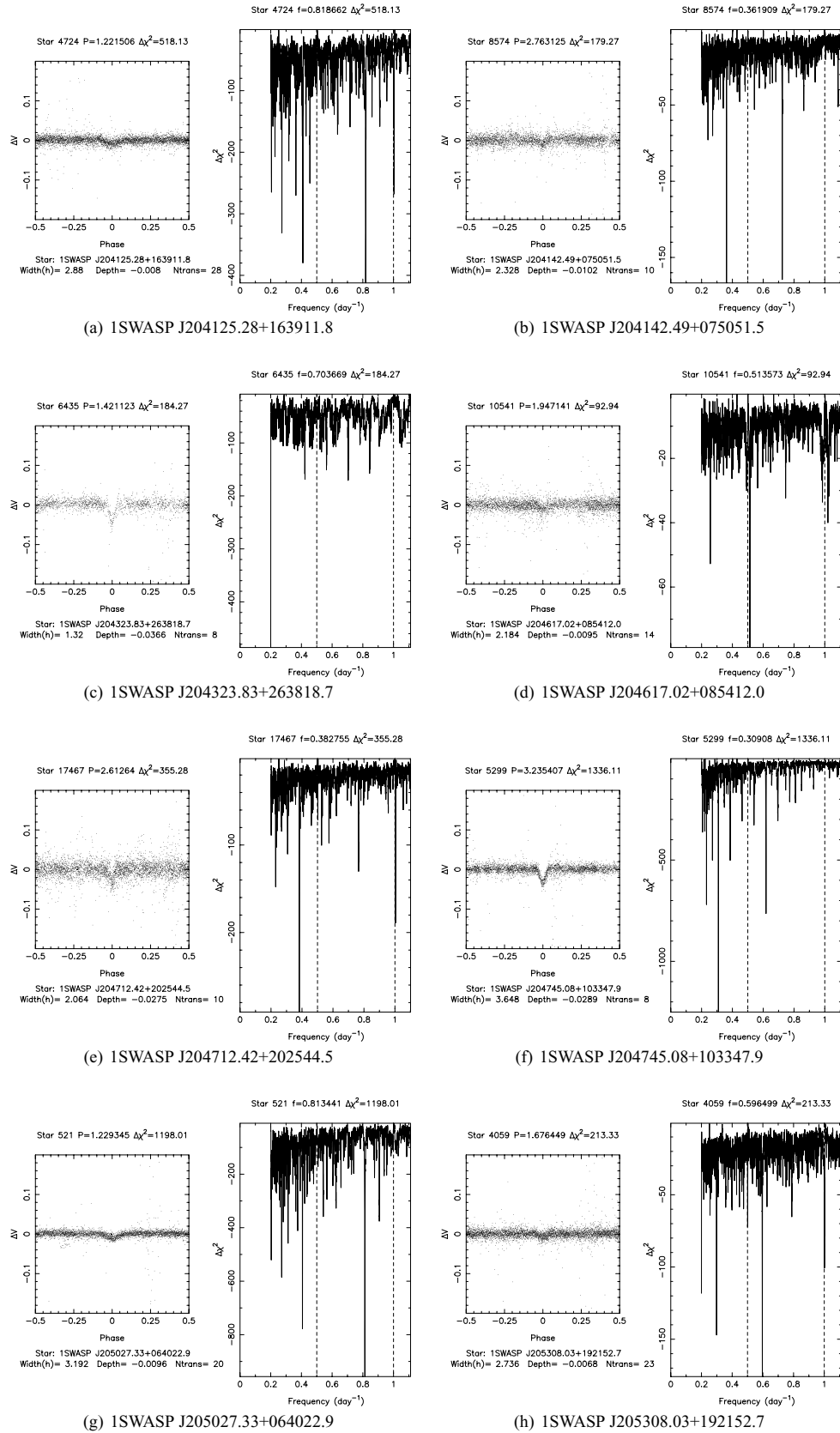
Figure 5. The light curves of the selected transit candidates, folded on the measured period.

(a) 1SWASP J210009.75+193107.1

(b) 1SWASP J210151.43+072326.7

(c) 1SWASP J210318.01+080117.8

(d) 1SWASP J210352.56+083258.9

(e) 1SWASP J210909.05+184950.9

(f) 1SWASP J210912.02+073843.3

(g) 1SWASP J211608.42+163220.3

(h) 1SWASP J211645.22+192136.8
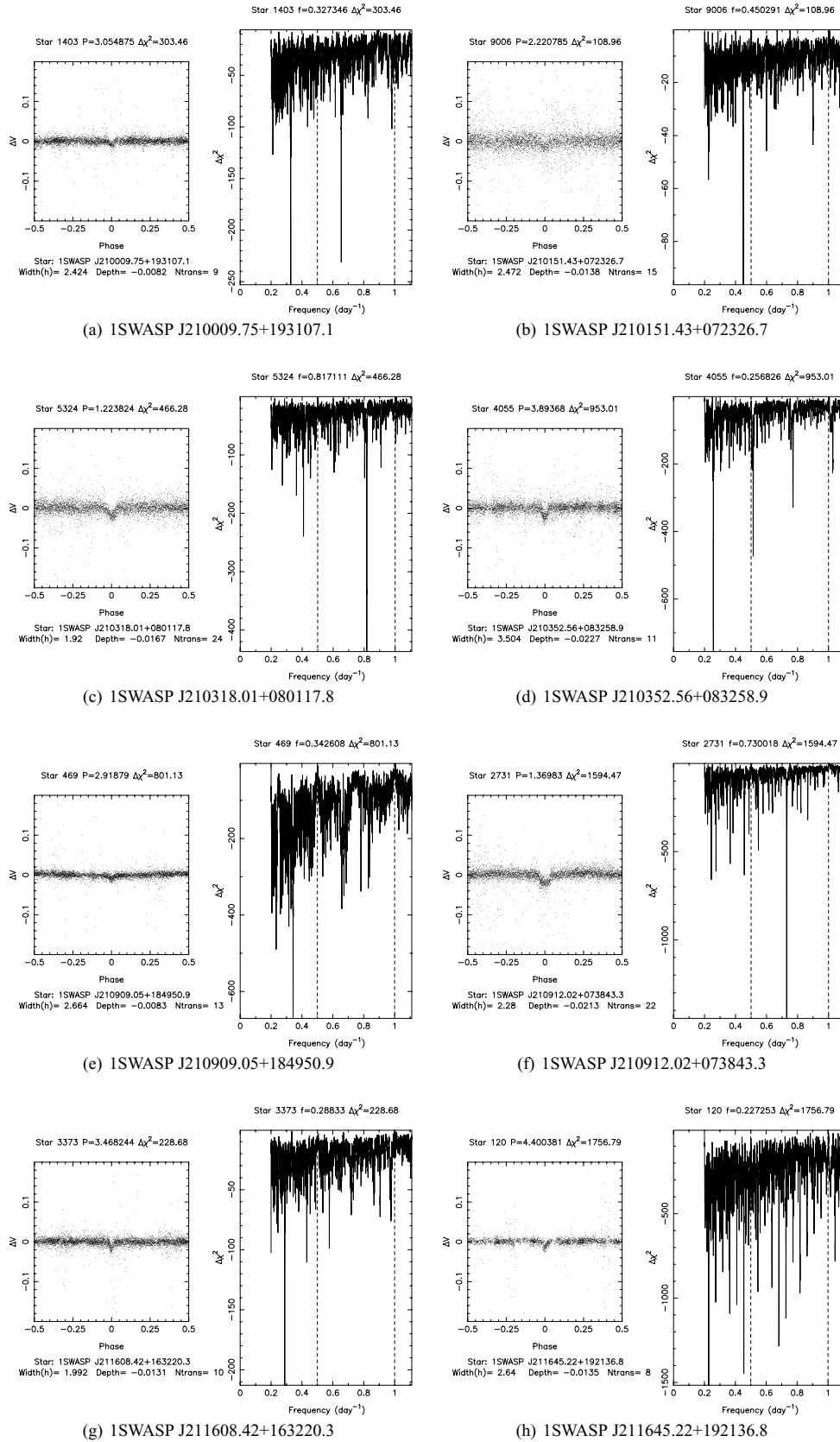
Figure 6. The light curves of the selected transit candidates, folded on the measured period.

(a) 1SWASP J212532.55+082904.4

(b) 1SWASP J212843.62+160806.2

(c) 1SWASP J212855.03+075753.5
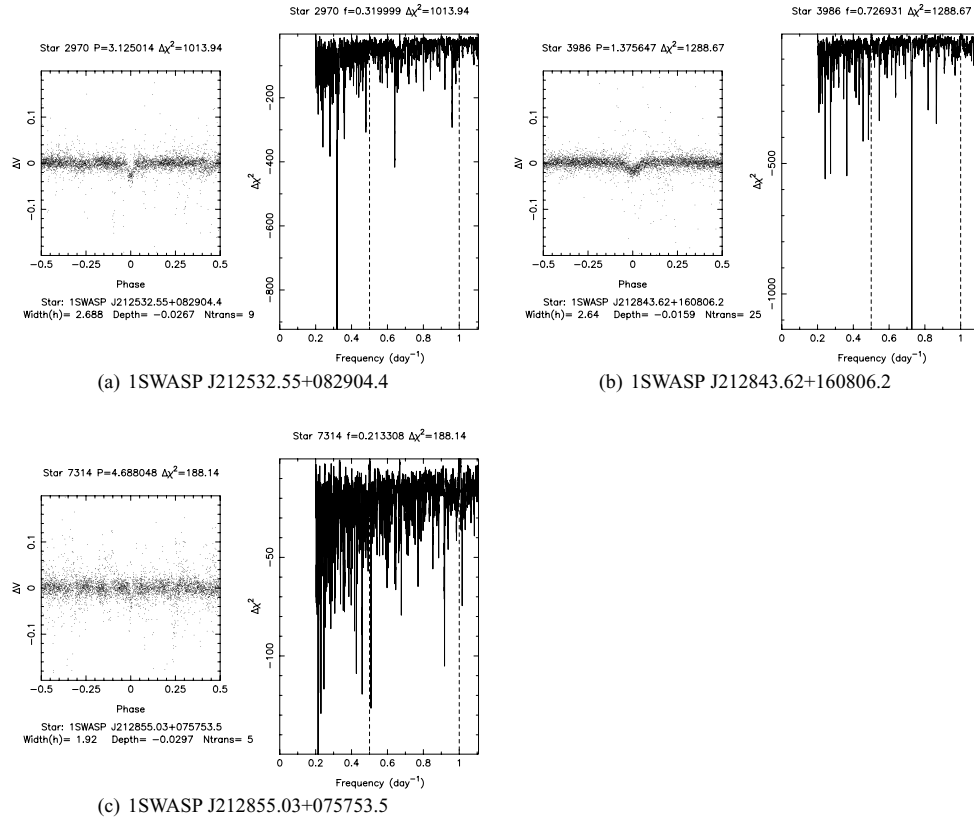
Figure 7. The light curves of the selected transit candidates, folded on the measured period.

acceptable η_p of 0.59. The few nearby objects raise the possibility of contaminating light but this remains a candidate.

4.13 1SWASP J203314.77+092823.4 and J203315.84+092854.2

These objects both display a similar periodicity at $P \sim 1.75$ d and are blended. It should be noted that J203315.84+092854.2 was actually eliminated at stage 3 since it has $S/N_{ellip} = 9.663$. This object was only retained because J203314.77+092823.4 passed the automatic criteria, but could not be considered in isolation. Both light curves are a little noisy and the transit has quite shallow in/egress slopes, but no other activity is apparent. The late spectral type of the former star makes this system interesting, implying a $0.94\,R_{Jup}$ companion radius but the $\eta_p = 1.59$ suggest the observed dips are longer than expected for a planetary object. The eclipses are more likely to be due to the latter object, an F2–F5 type, with a companion of radius $2.53\,R_{Jup}(\eta = 0.87)$.

4.14 1SWASP J203704.92+191525.1

The very low amplitude (9.5 mmag) and short (1.4 h) duration of this candidate makes the transit dips difficult to detect, but the signal is seen in the unfolded light curve and S-C periodogram. Obtaining follow-up photometry with a large telescope is therefore recommended. The predicted companion radius is close to that of Jupiter but the value of η_p is quite low, 0.55, implying that the observed transit duration is short compared with theoretical predictions. The target does have two other stars nearby so blending is a consideration.

4.15 1SWASP J203906.39+171345.9

Data points overlapping the clear transit-like dip indicated that the true period for this object was twice that found by HUNTER, i.e. 2.697 d. The 'V'-shape morphology then becomes clear in a flat, if noisy, light curve, and the predicted planet radius is only $1.35\,R_{Jup}$ with $\eta_p = 0.79$. This object is the brightest in a crowded field, and suffers from significant blending.

4.16 1SWASP J204125.28+163911.8

Despite the low amplitude of this candidate, visual inspection of the unfolded data confirms the occurrences of transit-like dips, and the S-C algorithm produces a strong spike at a frequency of 1/1.221 d. The predicted companion radius is extraordinarily low at $0.53\,R_{Jup}$ owing to the very red colour of the host star, which is classified as a mid-K type. The high value of η_p though, warns that the eclipse duration is longer than expected, and the star, while by far the brightest object in its field, does have nearby companions. Overall, we recommend this object for further investigation.

4.17 1SWASP J204142.49+075051.5

The low amplitude (10.2 mmag) and faint magnitude ($V \sim 12$ mag) of this object conspire to produce a very shallow transits of ~2.3-h duration. Their existence was confirmed by visual inspection however, and the strongest peak in the S-C periodogram corresponds to 2.763 d. Once folded on this period, the light curve shows no other form of variation from the mid- to late-K-type host star. The low predicted companion radius, $0.59\,R_{Jup}$, makes this an exciting

candidate, particularly in the light of the $\eta_p = 1.04$. Some nearby stars raise a caution of potential blending.

4.18 1SWASP J204323.83+263818.7

This star displays a clear 'V'-shaped dip when the light curve is folded on the period of one of the top five peaks, $P = 1.421$ d. Transits were observed of reasonable amplitude (0.04 mag) and fairly short (1.32 h) duration; however, there are hints of ellipsoidal variation and faint signs of secondary eclipses. The estimate radius for the companion object is a promising $1.32 R_{\rm Jup}$, though with a comparatively low $\eta_p = 0.63$, but this star has a very close companion and is certainly affected by blending. High-resolution imaging and/or spectroscopic observations are required to confirm or dismiss this candidate.

4.19 1SWASP J204617.02+085412.0

Another case where faint magnitude ($V \sim 12.3$ mag) and low amplitude (9.5 mmag) mask the transit signal, but close inspection reveals a series of shallow dips. The S-C periodogram is unclear, the period being so close to 2 d, but the folded light curve shows a transit-like dip in an otherwise flat data set. The G-type host star has one very close blended star, albeit a much fainter one as well as a group of other stars within the aperture, meaning the true companion radius could well be greater than the predicted $0.91 R_{\rm Jup}$. Nevertheless, we recommend this object for follow-up observations.

4.20 1SWASP J204712.42+202544.5

The faintness of this star (12.386 mag) leads to a noisy but apparently flat light curve except for a clear and credible transit dip. The host star's IR colour suggests a mid-K spectral type and a companion radius of $0.95 R_{\rm Jup}$, supported by the $\eta_p = 0.91$. Despite a number of much fainter companions, the level of blending is low in this field, strengthening the case for a planetary explanation in this case.

4.21 1SWASP J204745.08+103347.9

This is another case of a clear 'V'-shaped dip implying a stellar companion in spite of a low (~ 0.03 mag) amplitude in a light curve which shows no signs of ellipsoidal variation. The estimated companion radius of $1 R_{\rm Jup}$ is belied by a long transit duration ($\eta_p = 1.47$). The likelihood of blending in this case points to a stellar binary.

4.22 1SWASP J205027.33+064022.9

This bright ($V \sim 10.2$ mag) star displays a very shallow (9.6 mmag) but clear 'U'-shaped dip with an out of transit light curve that shows slight signs of ellipsoidal variation. The photometric precision is such that the transits are immediately obvious in the unfolded data. This is a good candidate, with a prediction companion radius of $0.92 R_{\rm Jup}$ though the transits are slightly longer than expected ($\eta_p = 1.43$). The star has two nearby companions of similar magnitude, so we have flagged it 'B' for a potential blend.

4.23 1SWASP J205308.03+192152.7

The very low amplitude (0.0068 mag) transit signal is just visible over the noise in this otherwise flat light curve but appears to exhibit a flat-bottomed dip. The amplitude means that despite a host star radius of $1.24 R_{\odot}$ the estimated companion radius is only $0.87 R_{\rm Jup}$,

supported by an $\eta_p = 1.04$. The five nearby stars means that contamination of the photometry cannot be ruled out without further observations.

4.24 1SWASP J210009.75+193107.1

This folded light curve displays a shallow but clear 'U'-shaped dip which can also been seen in the unfolded data. The periodogram exhibits a strong peak on the frequency 1/3.054875 although the period is close to an integer multiple of 1 d. The predicted radius implies a Jovian-sized companion, supported by an η_p of 0.71, but this object does suffer from blending.

4.25 1SWASP J210151.43+072326.7

At $V = 12.476$ mag, this is one of our faintest candidates, and the light curve has a commensurate level of noise, but transit-like dips can be seen in the unfolded data also and no other variability is visible in the light curve. The estimated companion radius of $0.92 R_{\rm Jup}$ is supported by $\eta_p = 0.99$. This star does have three nearby objects of similar brightness, and a much fainter object within ~ 4 arcsec, so blending is a possibility here.

4.26 1SWASP J210318.01+080117.8

This light curve shows a clear transit dip with believable width, depth and period and although the intrinsic noise makes the true morphology unclear there is no sign of any other variability. The measured duration is a close match for that predicted, and the companion radius of $1.01 R_{\rm Jup}$ makes this a strong candidate. A single nearby star raises a possibility of blending.

4.27 1SWASP J210352.56+083258.9

While noisy, this light curve clearly exhibits a ~ 0.02 mag dip and is flat out of transit though the relatively long period (close to the four times multiple of the 1-d alias) results in a certain amount of 'clumping' of data points. The $1.61 R_{\rm Jup}$ companion radius is on the borderline for a planetary companion, but is supported by an $\eta_p = 0.95$. Three nearby stars mean that the photometry for this object could be contaminated and that follow-up observations are necessary.

4.28 1SWASP J210909.05+184950.9

This bright ($V \sim 9.9$ mag) object shows a remarkably smooth light curve out of transit, allowing HUNTSMAN to detect the very shallow (8.2 mmag), 'U'-shaped transit dip. Closer inspection, however, reveals a marked ellipsoidal variation, flagging this object as a probable stellar binary. The host star is found to be of mid F-type yet the predicted companion radius is only $1.07 R_{\rm Jup}$, supported with an η_p of 0.71. While this object is certainly the brightest in its field, it is likely that nearby, fainter stars will have affected the SW-N photometry. We encourage follow-up observations of this target.

4.29 1SWASP J210912.02+073843.3

This star was included despite a high $S/N_{\rm ellip} = 12.508$ because the folded light curve appeared fairly flat to visual inspection, and showed clear, flat-bottomed transits with a duration of 2.28 h and $\delta = 0.0213$ mag appropriate for an exoplanet. The F-type host star implies a $R_p = 1.52 R_{\rm Jup}$ and $\eta_p = 0.89$. Further inspection reveals the object to be severely blended, so the true eclipses will be deeper.

As they are flat bottomed, the orbit must be edge-on. The companion could therefore be a low-mass star or brown dwarf and higher resolution photometry is recommended.

4.30 1SWASP J211608.42+163220.3

The brief dip in this flat light curve appears to be 'V' shaped, although intrinsic noise makes the morphology difficult to judge. The strong $\Delta\chi^2$ peak implies a credible period of 3.47 d. The estimated companion radius is Jovian at $1.18\,R_{\text{Jup}}$ though the low η_{p} of 0.59 implies the observed duration is shorter than predicted. As this star does not suffer from any blending it is a strong candidate for follow-up.

4.31 1SWASP J211645.22+192136.8

This object has a relatively long period of $\sim$4.4 d which means that a single observing station will normally only observe roughly one transit in two, weather permitting. For this reason there are some gaps in the light curve and, although a reasonable number of transits were detected, there is a higher degree of uncertainty on the period. This may explain the somewhat unclear transit curve. Nevertheless, this is a promising candidate: it is an isolated bright object, and the predicted companion radius is $1.23\,R_{\text{Jup}}$ with $\eta_{\text{p}} = 0.71$.

4.32 1SWASP J212532.55+082904.4

The transit signal is clearly visible in this slightly noisy light curve though the shape is not well defined. The companion radius is large but still within the planetary range at $1.58\,R_{\text{Jup}}$, backed up by an $\eta_{\text{p}} = 0.82$. There are no other stars close by this object, so it too is a target for further observations.

4.33 1SWASP J212843.62+160806.2

The folded light curve clearly shows a shallow dip of $\sim$0.02 mag with a believable period of 1.376 d. Closer inspection is needed to spot faint signs of a secondary eclipse and possible ellipsoidal variation ($S/N_{\text{ellip}} = 8.841$). The target has three objects nearby though all are $\geqslant$4 mag fainter. The late spectral type, derived from IR colours, leads us to suggest that this could be a low-mass binary.

4.34 1SWASP J212855.03+075753.5

The faintness ($V \sim 12.2$ mag) of this host star and the long period result in a low number of transits detected, and an under sampled, sharply 'V'-shaped signal in a noisy, but apparently flat, light curve. The nearby presence of a star of similar magnitude will also have contributed to the photometric uncertainty. The colour indicates a late G-type host star with a companion of radius $1.35\,R_{\text{Jup}}$, though the measured transit duration is shorter than expected for a planet ($\eta_{\text{p}} = 0.58$).

5 SPECTROSCOPIC CONFIRMATION OF CANDIDATE ASSESSMENT

While the analysis discussed above was at a preliminary stage, the opportunity arose to obtain echelle spectra of seven objects using the ESPaDOnS spectrograph on the Canada–France–Hawai'i Telescope (CFHT), Hawai'i, between 2005 September 23 and 24. These targets were taken from a preliminary selection list, according to the visibility from the telescope. The spectrograph was configured in spectropolarimetric mode during these observations, with a
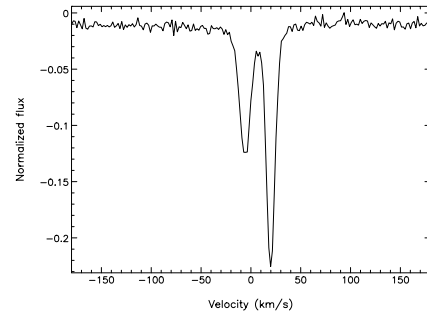

Figure 8. Deconvolved spectrum of 1SWASP J204456.57+182136.0 taken with ESPaDOnS at CFHT.

79 rules mm^{-1} grating achieving a resolution of $R \sim 68\,000$ and spanning over 40 orders in wavelength between 370 and 1050 nm. The filter in place was Stokes *I* band, and the exposure time was set between 300 and 600 s, depending on the magnitude of the target. These data were reduced at the telescope using the LIBRE-ESPRIT[3] online data reduction facility to perform the usual bias subtraction, flat-fielding and wavelength calibrations, followed by the order extraction of the polarization information.

Echelle spectroscopy provides a wavelength range of several thousand Angstroms and hence a large number ($n_l = 4688$) of images of a large sample (3507) of photospheric lines. These were used to boost the S/N of the spectra by a factor of by applying the least squares deconvolution method (see e.g. Donati & Collier Cameron 1997) in conjunction with a G2 line list. This analysis increased the S/N from $\sim$30 to $\sim$323. The telluric water lines within the echellogram were used to obtain a velocity calibration accurate to few $\sim$m s^{-1} of the heliocentric reference frame.

One of these stars, 1SWASP J204456.57+182136.0, falls within this data set. This object survived the selection procedure as far as the final stage, where it received a grade of 'CCB' because of a high companion radius estimate ($1.83\,R_{\text{Jup}}$) and $\eta_{\text{p}} = 1.79$. The low number of transits is a consequence of the long period ($\sim$8.15 d). Under our current selection procedure, this object was judged to be a blended stellar binary independently of the spectroscopic data. This assessment was confirmed by the CFHT spectra, shown in Fig. 8, which clearly shows a double-lined binary. These data give us confidence that our candidate selection procedure eliminates many astrophysical false positives, and prioritises strong exoplanet candidates for follow-up observations.

6 DISCUSSION

We have whittled down the original HUNTSMAN list of 11 626 stars observed within the RA range 18–21 h and have identified 35 objects of particular interest which we recommend for follow-up observations. We find six objects for which all the data currently at our disposal support the hypothesis that the companion object is planetary. These are summarized in Table 4. However, we encourage investigation of all these objects, since some narrowly missed the priority list, chiefly due to blending. In the tabulated data and discussions above we have noted any causes of uncertainty on a case-by-case basis. Furthermore, 'false alarms' from transit surveys provide a new sample of low-mass binaries, which are of interest in their own right.

[3]http://www.cfht.hawaii.edu/Instruments/Spectroscopy/Espadons/Espadons_esprit.html

Table 4. Priority exoplanet candidates.

Identifier 1SWASP. . .	Period (d)	Duration (h)	Depth (mag)	R_p (R_{Jup})
J183104.01+323942.7	2.378 781	1.776	0.0089	0.97
J184119.02+403008.4	3.734 014	4.224	0.0148	0.92
J204712.42+202544.5	2.612 64	2.064	0.0275	0.95
J210318.01+080117.8	1.223 824	1.92	0.0167	1.01
J211608.42+163220.3	3.468 244	1.992	0.0131	1.18
J211645.22+192136.8	4.400 381	2.640	0.0135	1.23

The SW-N instrument has proven to be an excellent way of finding transiting candidates among millions of bright field stars but it cannot conclusively determine the nature of these systems alone. As experience from a number of earlier transit surveys has shown (e.g. OGLE, Udalski et al. 2004; Vulcan, Borucki et al. 2001), a large (∼90 per cent) percentage of the candidates will turn out to be stellar binaries. Lister et al. (2006) estimate that ∼20–30 genuine exoplanets will be discovered in the 2004 season data as a whole, so we anticipate two–four to lie within this sample. This is an inescapable part of the nature of transit surveys: there are many astrophysical phenomena which mimic the signal of a transiting exoplanet (for a discussion, see Brown 2003; Charbonneau et al. 2004). Some of our candidates will be binary stars eclipsing at grazing incidence as seen from the Earth, others are likely to be binaries whose eclipses appear shallower than they are in reality because of light from a third object contaminating our photometry.

It is therefore necessary to execute a systematic and careful series of follow-up observations to finally establish the true nature of these objects, and in the process, accurately determine their physical and orbital parameters. We have an extensive program of photometric and spectroscopic follow-up on-going. We initially obtain one–two medium-resolution spectra of all priority candidates to confirm the spectral typing and hence the estimate of the minimum companion radius. These data will also eliminate single- and double-lined binaries and line-of-sight blends from the asymmetries in the line profiles. An imaging campaign running in parallel provides high-precision two-colour photometry at higher resolution around the times of transit of the best candidates. This can identify stellar companions from a detectable ($\lesssim$0.01 mag) difference in transit depth. Finally, the best candidates are subject to full radial velocity observations.

NOTE ADDED IN PRESS

Shortly after this paper was submitted, our follow-up program confirmed the planetary nature of the companion to the short-listed star 1SWASP J203054.12+062546.4, henceforth dubbed WASP-2b. For a detailed discussion of this discovery, see Cameron et al. (2007).

ACKNOWLEDGMENTS

REFERENCES

Ammons S., Robinson S., Strader J., Laughlin G., Fischer D., Wolf A., 2006, ApJ, 638, 1004
Borucki W. J., Caldwell D., Koch D. G., Webster L. D., Jenkins J. M., Ninkov Z., Showen R., 2001, PASP, 113, 439
Brown T., 2003, ApJ, 593, L125
Brown T. M., Charbonneau D., Gilliland R. L., Noyes R. W., Burrows A., 2001, ApJ, 552, 699
Burke C., Gaudi B., DePoy D., Pogge R., 2006, AJ, 130, 210
Burrows A., Guillot T., Hubbard W. B., Marley M. S., Saumon D., Lunine J. I., Sudarsky D., 2000, ApJ, 534, L97
Cabanela J., Humphreys R., Aldering G., Larsen J., Odewahn S., Thurmes P., Cornuelle C., 2003, PASP, 115, 837
Cameron A. C. et al., 2007, MNRAS, 375, 951
Chabrier G., Baraffe I., Allard F., Hauschildt P., Barman T., 2004, ApJ, 603, L53
Charbonneau D., Brown T., Noyes R., Gilliland R., 2002, ApJ, 568, 377
Charbonneau D., Brown T., Dunham E., Latham D., Looper D., Mandushev G., 2004, in Holt S. S., Deming D., eds, AIP Conf. Proc. Vol. 713, The Search for Other Worlds. Am. Inst. Phys., New York, p. 151
Charbonneau D., Brown T., Burrows A., Laughlin G., 2007, in Reipurth B., Jewitt D., Keil K., eds, Protostars and Planets V. Univ. Arizona Press, Tuscon, AZ, p. 701
Christian D. et al., 2006, MNRAS, 372, 1117
Collier Cameron A. et al., 2006, MNRAS, 373, 799
Cox A., 2000, Allen's Astrophysical Quantities, 4th edn. Springer-Verlag, Berlin
Donati J.-F., Collier Cameron A., 1997, MNRAS, 219, 1
Gray D. F., 1992, The Observation and Analysis of Stellar Photospheres, 2nd edn. Cambridge Univ. Press, Cambridge
Høg E. et al., 2000, A&A, 355, L27
Ipatov S., 1993, Astron. Vestn., 27, 83
Lin D. N. C., Bodenheimer P., Richardson D. C., 1996, Nat, 380, 606
Lister T. et al., 2007, MNRAS, in press (doi:10.1111/j.1365-2966.2007.11948.x)
O'Donovan F. et al., 2006, ApJ, 644, 1237
Perryman M. et al., 1997, A&A, 323, L49
Pollacco D. et al., 2006, PASP, 118, 1407
Pont F., Zucker S., Queloz D., 2006, MNRAS, 373, 231
Schwarzenberg-Czerny A., 1989, MNRAS, 241, 153 (S-C)
Schwarzenberg-Czerny A., 1999, ApJ, 516, 315 (S-C)
Skrutskie M. F. et al., 2006, AJ, 131, 1163
Smith A. M. S. et al., 2006, MNRAS, 373, 1151
Steffen J., Agol E., 2005, MNRAS, 364, L96
Tingley B., Sackett P., 2005, ApJ, 627, 1011
Udalski A., Szymanski M., Kubiak M., Pietrzynski G., Soszynski I., Zebrun K., Szewczyk O., Wyrzykowski L., 2004, Acta Astron., 54, 313
Vidal-Madjar A., Lecavelier des Etangs A., Désert J.-M., Ballester G., Ferlet R., Hébrard G., Mayor M., 2003, Nat, 422, 143
Vidal-Madjar A. et al., 2004, ApJ, 604, L69
Wenger M. et al., 2000, A&AS, 143, 9
Wilson D. et al., 2007, in Alfonso C., Weldrake D., Henning Th., eds, ASP Conf. Ser. Vol. Transiting Extrasolar Planets Workshop. Astron. Soc. Pac., San Francisco, p. 187

This paper has been typeset from a T$_E$X/L^{A}T$_E$X file prepared by the author.